Energies **2010**, *3*, 1914-1933; doi:10.3390/en3121914

OPEN ACCESS

energies

ISSN 1996-1073

www.mdpi.com/journal/energies

Article

Hybrid Dielectric-Metallic Back Reflector for Amorphous Silicon Solar Cells

James G. Mutitu *, Shouyuan Shi, Allen Barnett and Dennis W. Prather

Department of Electrical and Computer Engineering, University of Delaware, 151 Evans Hall Newark, DE 19716, USA; E-Mails: sshi@eecis.udel.edu (S.S.); abarnett@udel.Edu (A.B.); dprather@ee.udel.edu (D.W.P)

* Author to whom correspondence should be addressed; E-Mail: mutitu@eecis.udel.edu; Tel.: +1-302-690-5954; Fax: +1-302-831-4375.

Received: 19 November 2010 / Accepted: 8 December 2010 / Published: 10 December 2010

Abstract: In this paper, we present the design and fabrication of hybrid dielectric-metallic back surface reflectors, for applications in thin film amorphous silicon solar cells. Standard multilayer distributed Bragg reflectors, require a large number of layers in order to achieve high reflectance characteristics. As it turns out, the addition of a metallic layer, to the base of such a multilayer mirror, enables a reduction in the number of dielectric layers needed to attain high reflectance performance. This paper explores the design, experimental realization and opportunities, in thin film amorphous silicon solar cells, afforded by such hybrid dielectric-metallic back surface reflectors.

Keywords: solar cells; light trapping; amorphous silicon; back reflector

---

1. Introduction

In this era of uncertainty over the future of global energy as a whole, strong sentiments have arisen against the use and pursuit of fossil fuel sources. In the world at large, there is now a strong global push for stringent measures to reduce the amount of carbon emitted by every nation [1]. As a consequence, there has emerged a sudden and frantic rush for renewable energy solutions; with photovoltaic (PV) technology being one amongst many, in this endeavor.

At present, there is a constant drive to make PV competitive with other power production technologies, *i.e.*, to reduce final costs to less than 1 $/Watt [2,3]. This is where the world of thin film

solar cells (TFSC) comes to into play. Thin film technologies, reduce the material needed to make the solar cell, enable larger units of manufacturing than conventional wafer based technology and ultimately, are prime candidates for competitive power production. However, TFSC technologies suffer from one major problem, *i.e.*, lower efficiencies than conventional wafer based technologies [4].

The lesser efficiency is based on a number of reasons, one of which is that, with less material, there is less volume for the absorption of incident photons. This shortcoming leads to the need for optical light trapping; which is concerned with admitting the maximum amount of light into the solar cell and keeping the light within the structure for as long as possible.

Admitting the maximum amount of light into the solar cell is concerned with concepts of anti reflection, which are discussed in greater detail elsewhere [5–8]. The other problem, *i.e.*, keeping light within the cell, is where the focus of this paper lies. To trap light once it is inside a solar cell, the light needs to be scattered into the active material, reflected by a back reflector and ultimately prevented from coupling out of the structure. Information involving scattering light into the active material can be found in some of our previous work [6,7,9,10]. This paper is specifically concerned with the issue of back surface reflectance, and for that matter, finding a back reflector with fewer dielectric layers than standard distributed Bragg reflectors (DBR's). In Figure 1, we show a design schematic that summarizes the efforts of this study.

Figure 1. Design schematic showing the basic premise of the work presented in this paper. The idea is to find a high performance back surface reflector with few dielectric layers. The light is incident on the back reflector through a semi infinite a-Si structure.

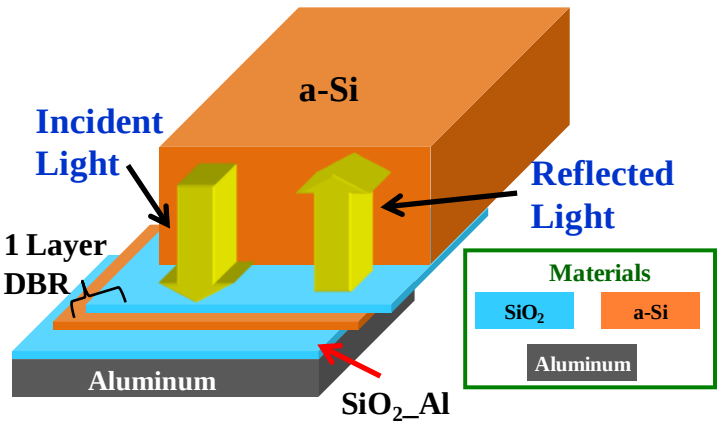

Our approach is purely from an optical perspective, and we chose to use amorphous silicon (a-Si) as the test material (active PV material), in this analysis. It is worthy to mention that the work in this paper is transferable to any other material using a similar approach. In the same light, since a-Si is mainly the test material, the issues relating to the electrical contacts are not addressed here. Contact formation in high performance a-Si solar cells is achieved using transparent conductive oxides (TCO) such as SnO_2 and ZnO. For back surface contacts, a thin layer of TCO is normally included between the a-Si and metal (mainly silver or aluminum); this is to prevent the formation of interfacial layers that can occur due to the reaction between the a-Si and metal [11]. The optical structure presented in this paper is transferable to some of the a-Si solar cell configurations that have been reported, such as

the one presented in [12]. More detailed accounts that specifically address TCO applications in a-Si solar cells can be found in the following references [12–16].

As with our previous work [6,9,10], we use the scattering matrix (S-Matrix) [17–19] and particle swarm optimization (PSO) [20–22], algorithms for the simulation process. To enable the achievement of high accuracy, during the simulation process, the optical material properties are acquired from actual materials, in our laboratory, using spectroscopic ellipsometry. This optical data is then input into the simulation code, resulting in models that greatly mirror real world performance.

2. Back Reflector Technology

Back reflectors in thin film solar cells, are of great value and importance. Especially when considering multiple passes of light through the solar cell structure, as is the goal of light trapping. However, the science of back surface reflectance is dictated by a number of important aspects, in addition to the reflective properties. These aspects include the back contact technology, material conductivity, passivation and the material adherence properties [12,16]. The combination of these features gives rise to a complex interplay, between the optical and electrical functionality. These requirements, often lead to the use of metals as back reflectors, because of their conductive and reflective material qualities. In practice, the quality of conductance and reflectance varies between metal and semiconductor materials; often the reflectance properties are substandard.

With the inadequate performance of metals as back surface reflectors (BSR's), and as the demand for higher and higher efficiencies increased, it became more apparent that different optical approaches were required. This led to the incorporation of photonic engineering concepts into the world of photovoltaics. In the span of a few years, we have witnessed the application of DBR's [23,24], 2D and 3D photonic crystals (PhC's) [25–27], diffraction gratings [28–30], plasmonic structures [31,32] and even the discovery of the worlds darkest materials [33–35]. It is apparent that there is a strong emergence of innovation in the world of photovoltaic photonics.

However, there is a major difference that exists between photonic engineering in photovoltaics and other semiconductor based technologies, which is the scale of the device structures. Solar cells are much larger than conventional microchip scale technologies. Furthermore, with the rise of thin film technologies, and subsequent industrial style large scale fabrication processes, such as roll to roll processing, the size of photovoltaic units has increased even further [2,3,16]. Therefore, even though photonic engineering concepts do significantly improve upon the light trapping capacity of solar cells, it is increasingly challenging for these concepts to find widespread applications. Thus, the problem in photovoltaic photonic engineering, involves increasing the optical light trapping properties, without exorbitantly increasing the overall cost of the PV unit. In line with these ideas, it was the aim of this study, to find a good back reflector that requires only a few dielectric layers of material, and hence, not requiring very complex fabrication processes to realize.

3. Design Process

With all this in perspective, we now begin to look specifically at BSR's. In some of our earlier work on light trapping, we found that the introduction of a metallic layer, at the base of a 6 layer 1D-PhC, increased the overall reflectance of the structure [6,7,9]. This observation led us into the realm of

hybrid dielectric-metallic reflectors and their potential application in photovoltaic devices. We were trying to find out the number of dielectric layers that are actually necessary, to make a good back reflector for a solar cell structure.

The first step in the study, was to figure out what thickness of our chosen solar cell material, a-Si, would be ideal for the back reflector analysis. On inspection of the absorption coefficient data for a-Si, it is evident that most of the incident light energy is absorbed within the first three hundred nanometers of an a-Si structure [16]. However, many of the papers on a-Si solar cells, have the active layer thicknesses ranging from a few hundred nanometers to a number of microns [12–14,25,36]. With there being such great variation in the choice of active layer thicknesses, we decided to perform a fundamental analysis on the absorption characteristics of a-Si structures, as is shown in Figure 2a. In the figure the numbers that correspond to each plot in the figure legend, denote the thickness of the a-Si structure.

The basic idea of the study was to use simulations to aid in observing the absorption characteristics of a-Si structures of varying thickness (from 100 nm to 2 μm). In the simulation, the a-Si structure being analyzed was placed between two semi infinite slabs of a-Si. In this way, we could observe how much light is absorbed in a single pass through an a-Si structure; without any front surface reflection or any light trapping.

We observed that, at a thickness of about 500 nm for the a-Si layer, the absorption curve began to fall off from the maximum, at a value close to the 600 nm wavelength point; which is the midpoint of the wavelength range under consideration (400–800 nm). In addition, the distance between the absorption curves, becomes remarkably small after the 500 nm thickness. Also, the 500 nm thickness, is in line with other optical studies performed on a-Si solar cells [12,25,37].

After obtaining an appropriate active layer thickness of 500 nm, we proceeded to analyze the transmission characteristics of the structure, as shown in Figure 2b. The transmission characteristics show us what wavelengths actually hit the back reflector and hence, give us a clearer picture of our design space. As is seen in Figure 2b, the transmission of light begins at a wavelength of close to 600 nm. Therefore, we set the design wavelength range for the back reflector as 600–800 nm.

Figure 2. (a) Absorption characteristics of a-Si structures of different thicknesses; (b) Transmission characteristics of the structures. In both (a) and (b), the curve for the 500 nm thick structure is bolded.

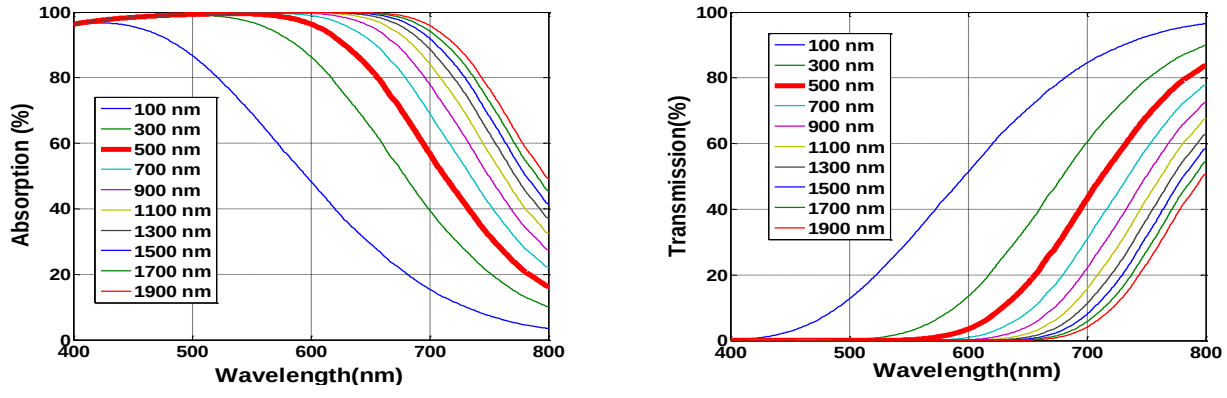

(a) (b)

The next step in the study is summarized in Figure 3; we wanted to compare various back reflector structures for a-Si solar cells, with the hope of coming up with a structure with very few dielectric layers. We simulated the reflectance characteristics of a semi-infinite a-Si structure atop an aluminum only layer, Figure 3a, a multilayer DBR, Figure 3b, and a hybrid dielectric-metallic structure, Figure 3c. In the multilayer DBR, we varied the number of periods from one to five, using the name, "1 Layer" to denote a structure with one period, "2 Layer" for a structure with two periods, and so on. There is an added phase matching layer in Figure 3c, denoted by SiO_2_Al, in addition to the 1 Layer DBR and aluminum layer.

Figure 3. Schematic of an a-Si structure atop, (a) an aluminum reflector, (b) a standard multilayer DBR structure with a large number (N) of layers, (c) a reduced layer, hybrid dielectric-metallic back reflector.

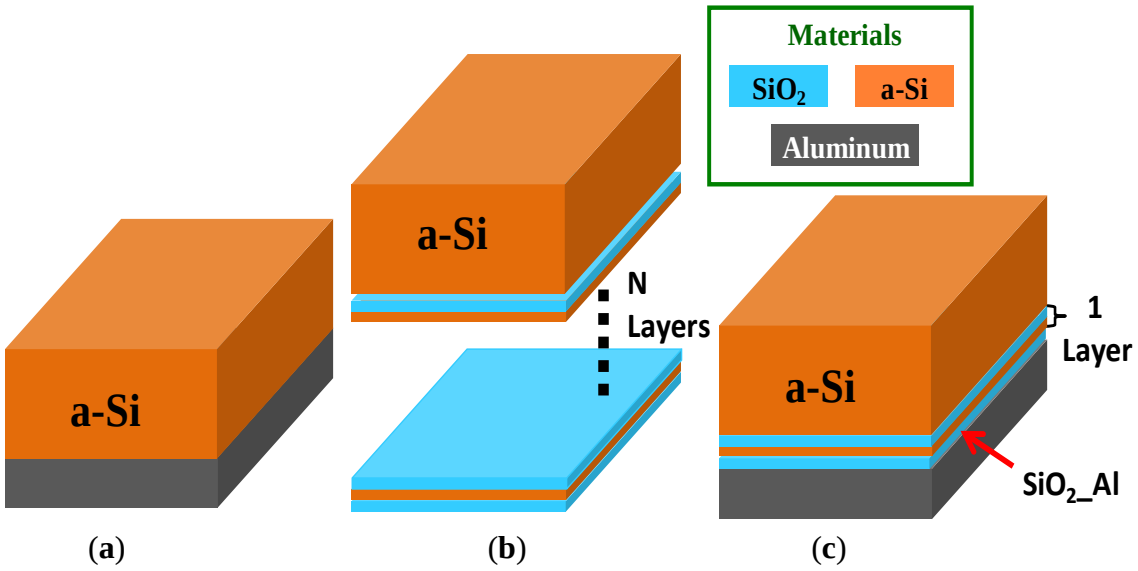

To obtain the highest reflectance for the desired wavelength range, 600–800 nm, we employed the use of our optimization algorithm, PSO. This work was performed in order to obtain the optimal design parameters, for a varying number of periods in a distributed Bragg reflector stack. Each DBR stack was set atop a SiO_2 substrate and had a semi infinite a-Si superstrate (cladding layer), the results of the reflectance study are shown in Figure 4. It can be observed that only about three layers are needed to achieve a reflectance that is similar to that of a stack with many more layers. The difference between the "3 Layer" and "5 Layer" structure, in terms of percentage reflectance, in the 600–800 nm range, is 0.5%. With this observation in tow, the next step was to observe the reflectance characteristics of the DBR structures after the addition of a metallic layer, *i.e.*, the performance of the hybrid dielectric-metallic BSR.

Figure 4. Reflectance characteristics for DBR's with a varying number of layers, the label "1 Layer" is used to denote a DBR with one period, "2 Layer" for a DBR with two periods, and so forth.

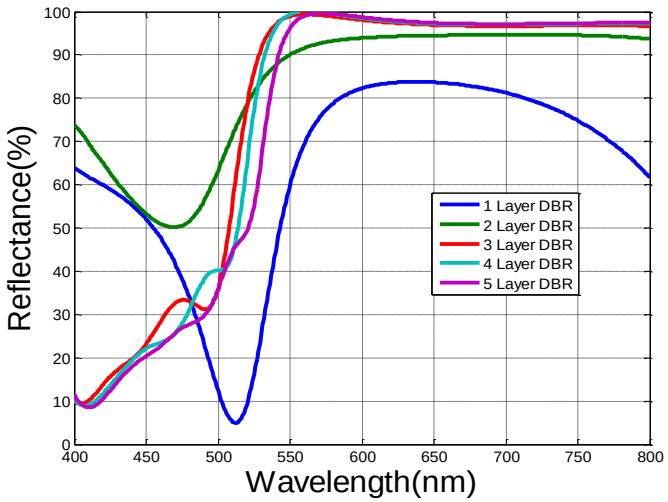

We chose to use aluminum as the metallic layer, because of its widespread use in the PV industry. Aluminum has been used for a long time as a back reflecting material in many types of solar cells. As a matter of fact, for a long time it was assumed that metals were really good BSR's and most optical analysis considered any metallic material used as a perfect electrical conductor. However, it came to be understood that the "parasitic" absorption characteristics of aluminum, especially in a-Si solar cells, is very significant [37]. As was concluded in various studies [37–39], the addition of a phase matching layer to separate the metal from the semiconductor or multilayer stack, significantly reduces the amount of light that actually gets absorbed in the metal layer. Following this train of thought, we introduced a layer of SiO_2 between an aluminum and DBR stack, and subsequently employed optimization to figure out the thickness of this layer. This optimization was performed for each of the structures that were analyzed in Figure 4. The resultant reflectance characteristics are shown in Figure 5.

Figure 5. Reflectance characteristics for structures with the different number of DBR layers, with an added SiO_2 phase matching layer and aluminum layer.

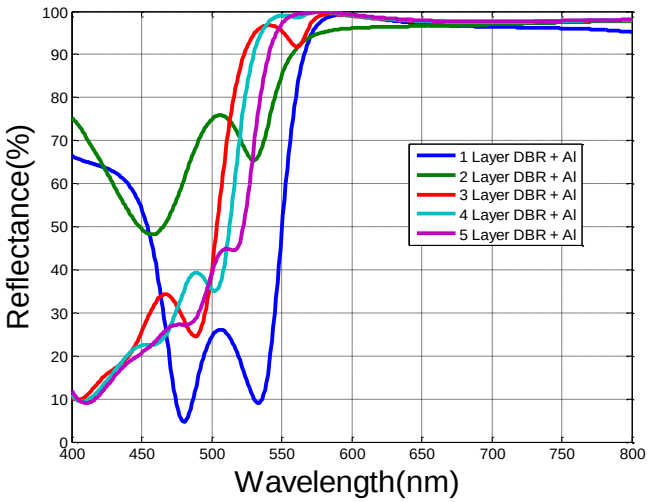

As can be seen in Figure 5, the reflectance characteristics of the various structures, in the region of interest (600–800 nm), are quite similar. We see, from Figure 5, that even the structure with one DBR period, has a very high reflectance. For that matter, the three period DBR stack, has a reflectance that is almost identical to that of the 4 and 5 period DBR structures. Of greater interest is the 1 Layer DBR structure, which has a reflectance of 97.7% (600–800 nm). Even though the reflectance is about 1.1% less than that of the 3 period stacks, the number of layers is fewer.

In order to provide clarity on the various naming conventions used, we illustrate the one period structure (1 Layer DBR) and 3 period structure (3 Layer DBR), as shown in Figure 6.

Figure 6. Design schematic of the, (a) 1 Layer DBR and, (b) 3 Layer DBR structures. The SiO_2 (DBR:SiO_2 Layer) and a-Si (DBR:a-Si Layer) layers of the DBR structures are labeled. The phase matching SiO_2 layer (SiO_2_Al) and the aluminum layer are also shown.

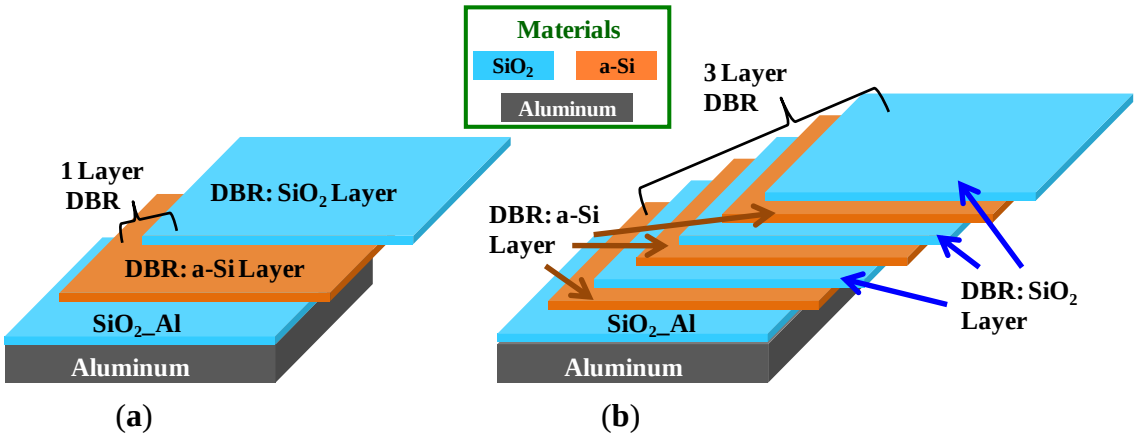

This naming convention is the same for all structures that are presented in this manuscript. The SiO_2 layers of the DBR are called DBR:SiO_2 and the a-Si layers are labeled DBR:a-Si, the phase matching layer is labeled SiO_2_Al. The design parameters for these layers, in the 1, 2 and 3 Layer DBR structures are presented in Table 1.

The amount of light absorbed in the BSR is minimal, as can be seen by the high reflectance values of the various structures in Table 1. These results show us that the absorption, in the otherwise lossy metal, is mitigated by the addition of the dielectric layers, and in turn, the metal increases the overall reflectance.

Table 1. The design parameters and performance characteristics of the 1, 2 and 3 layer DBR structures, are presented.

Structure	DBR:SiO_2 Layer (nm)	DBR:a-Si Layer (nm)	SiO_2_Al (nm)	Avg Reflectance (%) (600–800 nm) no metal	Avg Reflectance (%) (600–800 nm) with Aluminum
1 Layer DBR	345	36	147	80	97.7
2 Layer DBR	118	38	150	96	98
3 Layer DBR	137	32	172	98.4	98.8

The absorption in the entire BSR, Abs_{BSR}, can be calculated by subtracting the percentage reflectance, Ref_{BSR}, and transmittance, $Trans_{BSR}$, from 100%, as is shown in Equation (1). The resultant absorption for the 1 layer structure with no metal is 2% (600–800 nm), and 2.3% with the addition of the aluminum layer. This means that the addition of the aluminum layer increases the back reflector losses by 0.3%, in the 600–800 nm range.

$$Abs_{BSR} = 100 - Ref_{BSR} - Trans_{BSR} \quad (1)$$

To put the performance of the 1 Layer DBR into context, we plot the reflectance characteristics of an aluminum layer, a 1 Layer DBR and a 1 Layer DBR with an added aluminum layer, as is shown in Figure 7. These structures reflect the light into a semi infinite a-Si cladding layer (layer on top of reflector). The benefits of adding the aluminum layer to the 1 Layer DBR are clearly visible, especially in comparison to the reflectance characteristics of the plain aluminum layer. The reflectance, in the 600–800 nm range, of the aluminum only structure is 66%, that of the one period DBR stack is 80%, and that of the 1 Layer DBR with the added aluminum layer is 97.7%.

Finally we perform a tolerance analysis of the 1 Layer DBR structure by altering the dimensions of the parameters, by ±5%, ±10% and ±15%, as shown in Figure 8. We slightly increase the bandwidth to 590–800 nm, to further give an idea of the robustness of the reflector. As is seen in Figure 8, the reflectance characteristics stay above 90%, for a design tolerance of 0% to −15%. In the positive direction, we see that the reflectance is more affected at the extremity, +15%, where the reflectance drops to about 86%. All in all, the reflectance values stay above 90%, in the tolerance range of −15% to about +12%.

Figure 7. Reflectance characteristics of the 1 layer DBR structure (green plot), as compared to a structure of aluminum only (blue plot), and one with the 1 layer DBR plus an aluminum layer (red plot).

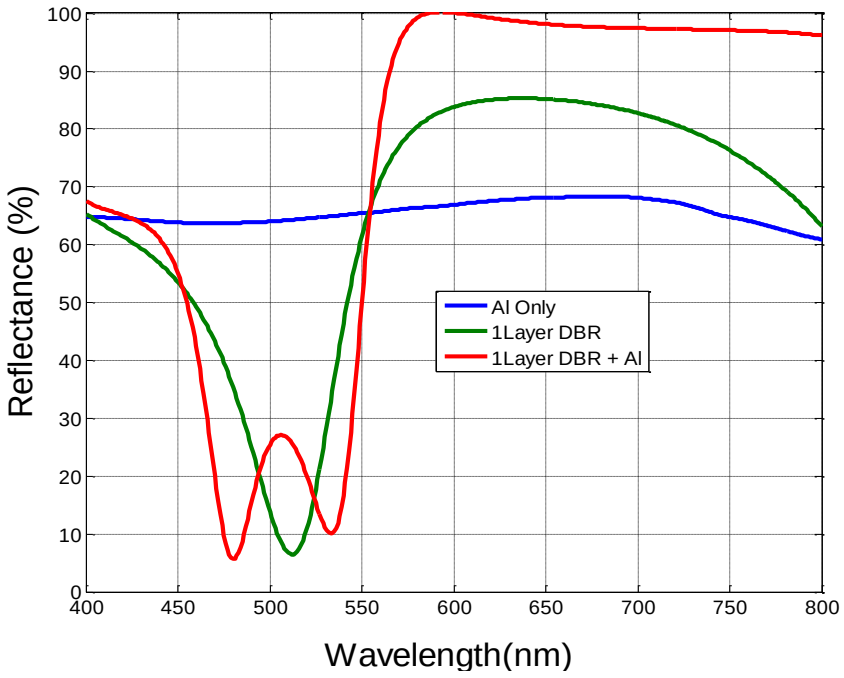

Figure 8. Tolerance analysis of the design parameters of the 1 Layer DBR structure with an added aluminum layer.

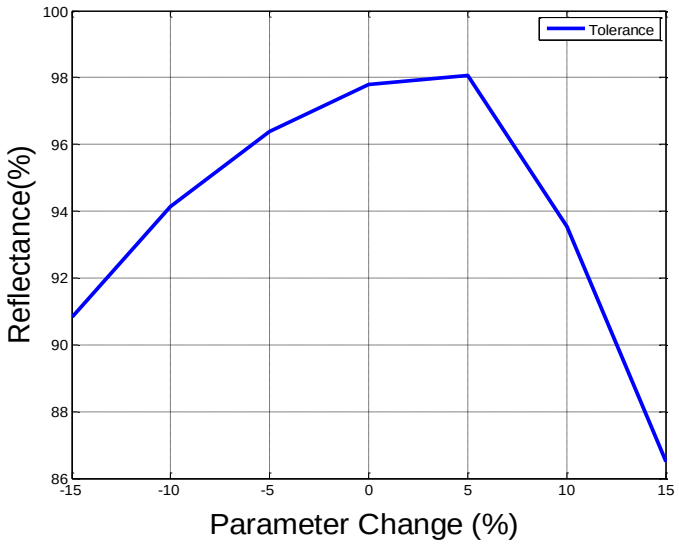

The governing physical behavior of the hybrid dielectric-metallic back reflector can be described using the theory of reflection and transmission of light waves at multiple interfaces, as is depicted in Figure 9. If we consider a light wave, T_1, that is incident through the a-Si active layer, as is shown in Figure 9, we observe that as it impinges on the first SiO_2 layer in the DBR, a portion of the incident power, R_1, gets reflected and the rest, T_2, is transmitted. The exact magnitudes of R_1 and T_2 can be deduced using Fresnel formulae, which are described in great detail in [5,38–40]. The wave reflected off the n_1/n_2 interface, R_1, does not experience a phase change, since $n_1 > n_2$.

Figure 9. Diagram showing the propagation of a wave through the stratified 1 layer DBR + aluminum back reflector. The wave undergoes multiple reflections as it moves from one medium to the next. The corresponding phase change on reflection, the refractive indices and thicknesses of the individual layers are shown.

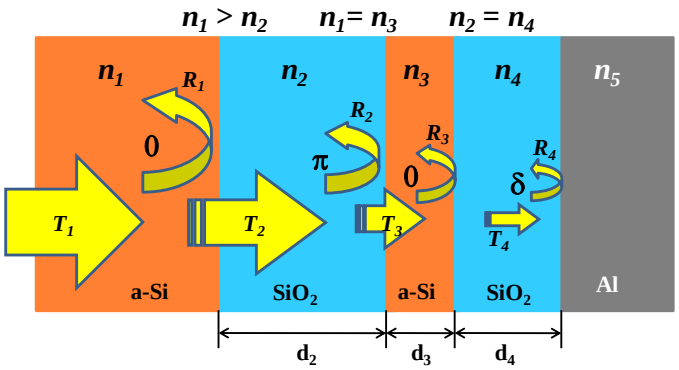

The transmitted wave, T_2, traverses through the SiO_2 layer and onto the n_2/n_3 interface, where again part of it is reflected, R_2, and the rest transmitted, T_3. Since $n_2 < n_3$, R_2 experiences a π phase shift on reflection at the n_2/n_3 interface. As R_2 travels through the SiO_2 layer, a distance of $2d_2$, it picks up a roundtrip phase shift, in addition to the π phase change on reflection from the n_2/n_3 interface. Therefore, the relative phase shift of the two reflected waves, *i.e.*, R_1 and R_2 is given by the difference

between the change in phase experienced by R_1 and the total roundtrip phase change experienced by R_2 (which includes the π phase shift from the n_2/n_3 interface). If this relative phase difference is an integral number of wavelengths, then constructive interference occurs.

The portion of wave that hits the back aluminum layer experiences a phase change that is not quite equal to π because of the lossy nature of the metal, $\delta < \pi$ for all wavelengths [39]. Hence the need for a layer that ensures that the waves reflected off the n_3/n_4 and n_4/n_5 interfaces are in phase, *i.e.*, R_3 and R_4 are in phase. This layer is the phase matching layer which is depicted in Figure 9, as having a thickness of d_4; it is referred to as SiO_2_Al in the rest of this manuscript.

At this juncture, it is worthwhile to mention that most analytical treatments that provide optimal parameters for the maximum reflectance of such an arrangement, consider mainly single or small wavelength bands [8,38]. In practice however, when considering broadband illumination, such as sunlight, we need to use optimization algorithms and electromagnetic simulation tools to obtain the optimal design parameters. To this end, we employ the particle swarm optimization and S-Matrix algorithms to optimize the design parameters over the entire wavelength region of interest.

It is also important to show the optical constants used in this study. To this end, we plot the real part of the refractive index, *n*, in Figure 10a, and the absorption coefficient for aluminum and a-Si in Figure 10b.

The next step in the analysis was to experimentally realize the design structures through fabrication processes. We chose to analyze a structure that incorporates the 1 Layer DBR, as it has shown high performance in simulation.

Figure 10. (a) Refractive index, *n*, of the different materials used in the back reflector; (b) log plot of absorption coefficient data for the a-Si and aluminum materials used in the study.

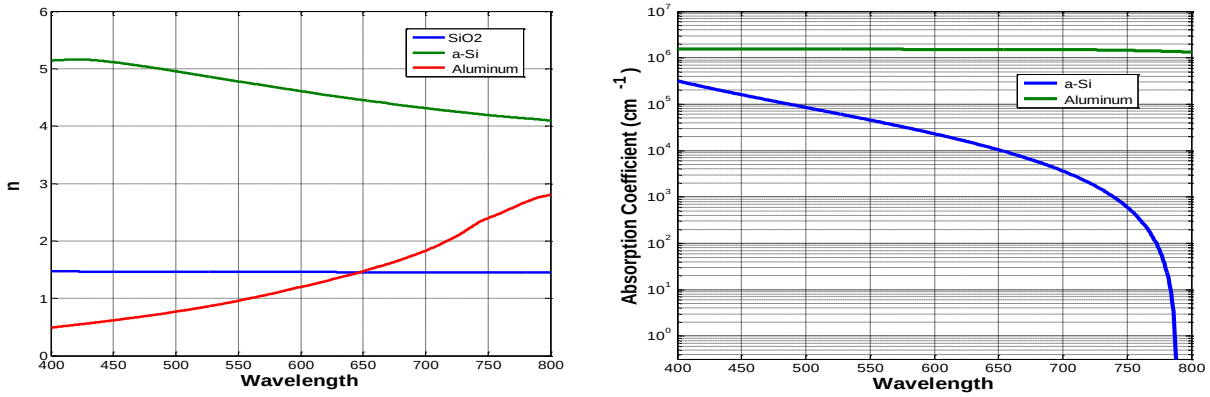

(**a**) (**b**)

4. Fabrication Results

We fabricated four structures; the first, which we will refer to as "a-Si Only", consisted of a single layer of a-Si, deposited on a glass slide. The second structure had an anti reflection coating (ARC), added to an a-Si layer, and we refer to this structure as "ARC + a-Si". The third structure, incorporated the ARC and 1 layer DBR, we refer to this structure as "ARC+a-Si+1 Layer". Finally, the last structure had the ARC, the 1 layer DBR and the aluminum layer; we refer to this structure as

"ARC + a-Si + 1 Layer + Al". All the design parameters, for all the various components, of the four structures are specified in Table 2. A design schematic of the fourth structure, *i.e.*, the structure with an ARC, 1 Layer DBR and aluminum layer, is shown in Figure 11.

These structures were all fabricated on glass slides. In the structures which incorporated an aluminum layer, the aluminum was deposited first, on the glass slide, using electron beam evaporation. All the other layers were deposited on top of the aluminum layer, using plasma enhanced chemical vapor deposition (PECVD). The structures that had no aluminum were directly deposited on the glass slides using PECVD. The configuration of these structures corresponds to the "substrate" optical design, where sunlight enters the solar cell before it reaches the substrate, which is outlined in [16].

Table 2. Summary of optimal design parameters for the fabricated solar cell structures.

Structure	Design Parameters (in nm)
AR coating (SiO_2)	10
AR coating (Si_3N_4)	62
a-Si active layer	500
1 Layer DBR (SiO_2)	345
1 Layer DBR (a-Si)	36
SiO_2_Al	147
Aluminum Layer	4000

Figure 11. Design schematic of the structure that was fabricated. The structure incorporates an AR coating, a 1Layer (1 period) DBR, a SiO_2 phase matching layer (SiO_2_Al) and an aluminum layer, all deposited on a glass slide.

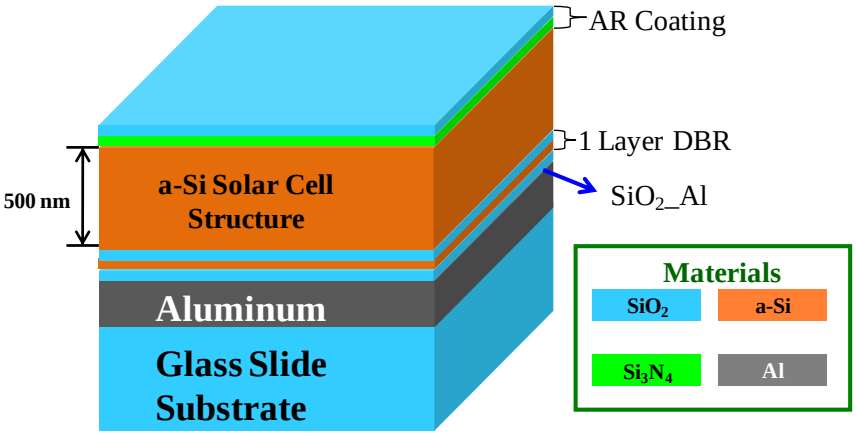

We also simulated the structures with the design parameters listed above and attained graphs, showing the absorption characteristics, as shown in Figure 12. As the back reflectors are added, we see the presence of Fabry-Perot resonance peaks, which occur at wavelengths described in the following equation.

$$\lambda_m = \frac{2nt}{m} \tag{2}$$

where n is the refractive index, and t is the thickness of the active solar cell material (a-Si), and m is an integer [5,8].

Figure 12. Simulation of absorption characteristics of the different structures. The first structure has no light trapping (blue plot), the second incorporates an AR coating (green plot) , the third has the AR coating and the one layer DBR (red plot), the final one has the AR coating, 1 Layer DBR and the aluminum layer (purple plot).

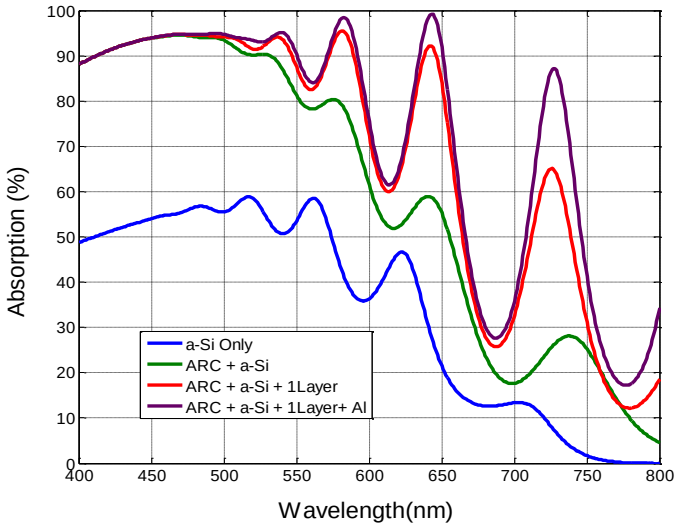

We characterized the reflection and transmission characteristics of the fabricated structures, using a spectrophotometer that is fitted with an integrating sphere. To calculate the absorption, we used an equation similar to Equation (1), only this time, the absorption, reflection and transmission characteristics, are for the fabricated structures, which all included a 500 nm a-Si layer. We tabulate the corresponding average absorption (400–800 nm) values in Table 3, and plot the absorption characteristics, in Figure 13.

Figure 13. Absorption characteristics for the different fabricated structures. The first structure has no light trapping (blue plot), the second incorporates an AR coating (green plot), the third has the AR coating plus the one layer DBR (red plot), the final plot has the AR coating, 1 Layer DBR and the aluminum layer (purple plot).

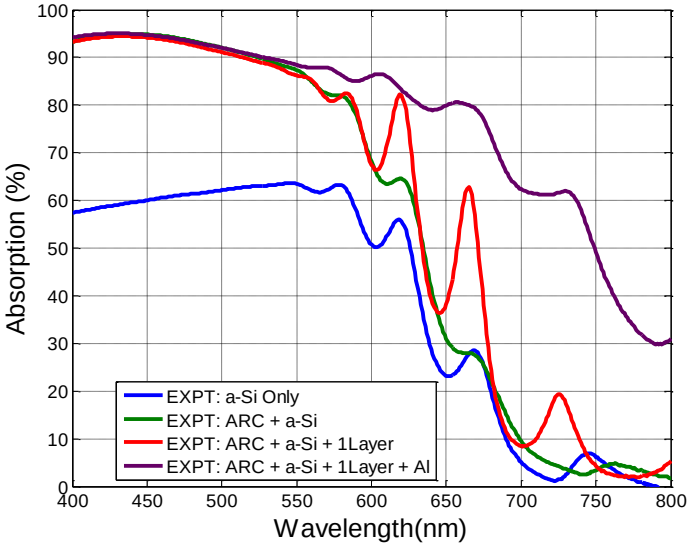

Table 3. Final values of the average absorption for different structures over the entire 400–800 nm range.

Structure	Avg. Absorption (%) Simulation	Avg. Absorption (%) Experimental
a-Si Only	38	41
ARC + a-Si	63	58
ARC + a-Si + 1 Layer	71	61
ARC + a-Si + 1 Layer + Al	76	80

5. Discussion

The absorption characteristics of Figure 13 show a number of physical phenomena that are worth noting. With the addition of the 1 layer DBR, corresponding to the red plot in Figure 13, we see clearly accented absorption peaks at 620, 670 and 725 nm. The peaks correspond to resonance frequencies, due to the fact that the planar a-Si layer, with a reflector on one side, forms a Fabry-Perot etalon. The addition of a better reflector at the back surface serves to increase the height of the peaks, at the same wavelengths. In the plot with the metal added, the purple plot in Figure 13, we see that the increased peaks are present; however the graph has been "smoothened", as compared to what we would expect. We do not see the drastic dips in absorption that show up in the simulation results of Figure 12.

To account for this discrepancy, we took a closer look at the structures we had fabricated using a scanning electron microscope. We saw that the structures without any aluminum were mostly planar; however, the samples with the aluminum layer had a very rough surface morphology, as is shown in Figure 14.

Figure 14. SEM images of the surfaces of (a) the planar structure with an AR coating and 1 period DBR at the back; the image shows a bit of the edge of the sample and the top surface, which reveals how planar the surface is, and (b) the structure with an AR coating, 1 period DBR and an aluminum layer. The roughness in the aluminum is carried through to the entire structure and hence the bumpy surface.

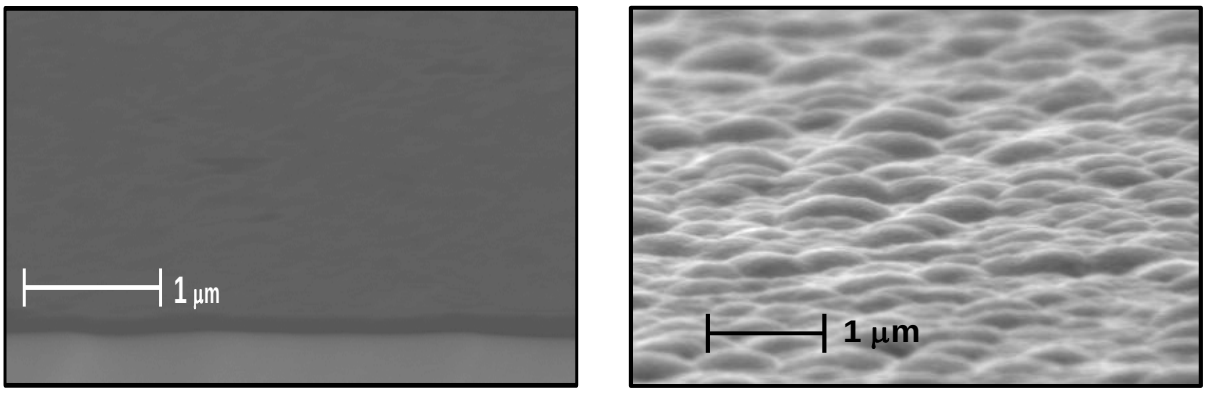

(**a**) (**b**)

After this observation, we incorporated roughness into the simulation code by altering the design geometry of the structure, by including bumps; which mimic the ones shown in the SEM image. Since the bumps, as shown in the SEM image, were of arbitrary sizes, we included bumps that varied in size

into the simulation code. We varied the height of the bumps from 70 nm to about 150 nm, with steps of 25 nm in between. As for the width, we varied the size from 100 nm to about 700 nm, with steps of 100 nm in between. We had observed, in the SEM images that the roughness began from the surface of the deposited aluminum, and hence in the simulations we incorporated the bumps into the aluminum layer, DBR layer, a-Si active layer and AR coating layer. Hence, in essence, the roughness that began at the aluminum layer translated throughout the rest of the structure.

We then took the average of the results from all the simulations and got the simulation plot shown in Figure 15. There was a much better match between this simulation results, with roughness, and the fabrication results, than with the previous simulations that did not incorporate roughness (Figure 12). The simulation result, with roughness, and the fabrication results are compared in Figure 15 and Table 4. We can clearly observe that the accuracy of the method of simulation with roughness is much higher than that without roughness. Hence we were able to conclude that the aluminum layer introduced some roughness, which translated throughout the structure, and in turn improved the absorption characteristics from what we had earlier anticipated through simulation.

Figure 15. Absorption characteristics for the structure with an AR coating, 1 Layer DBR and aluminum layer. The graph compares the experimental results (purple plot), with the simulation results that incorporate roughness (blue plot).

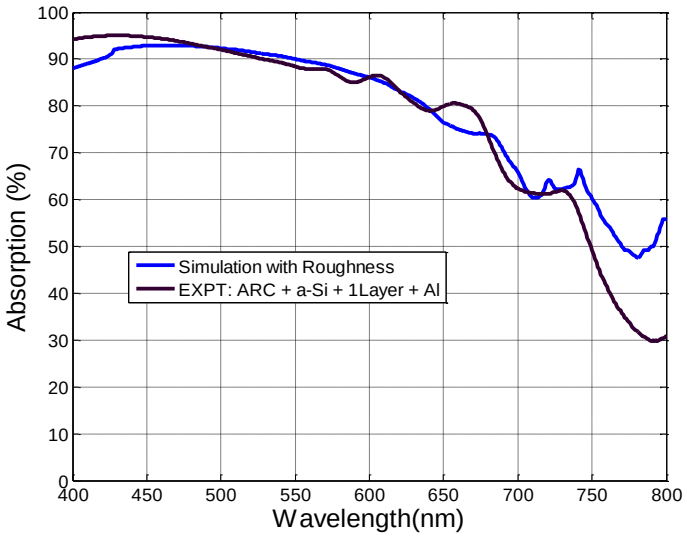

Table 4. Final average absorption values for the structure with an ARC, 1 Layer DBR and aluminum layer. The table compares the experimental results with the simulation that incorporates roughness.

Structure	Avg. Absorption (%) Simulation with Roughness	Avg. Absorption (%) Experimental
ARC + a-Si + 1 Layer + Al	80.2	80

As with our previous analysis [9,10], we computed the enhancement factor; which is a comparison of the absorption characteristics of the modified structures, to those of a structure with no light trapping enhancement (a-Si only), as shown in Equation (3).

$$EF(\lambda) = \frac{\int_{\lambda}^{\lambda=800} A_{\mathrm{E}}(\lambda')Irrd(\lambda')\mathrm{d}\lambda'}{\int_{\lambda}^{\lambda=800} A_{\mathrm{S}}(\lambda')Irrd(\lambda')\mathrm{d}\lambda'} \quad (3)$$

where the value A_{E} represents the absorption characteristics of an enhanced structure, *i.e.*, with light trapping incorporated, A_{S} represents the absorption of a structure with no light trapping, *i.e.*, the a-Si only structure.

We then plotted the enhancement factor characteristics from 600–800 nm, for this is where the characteristics are most strongly observed, as is shown in Figure 16.

Figure 16. Enhancement factor comparison of the different fabricated structures.

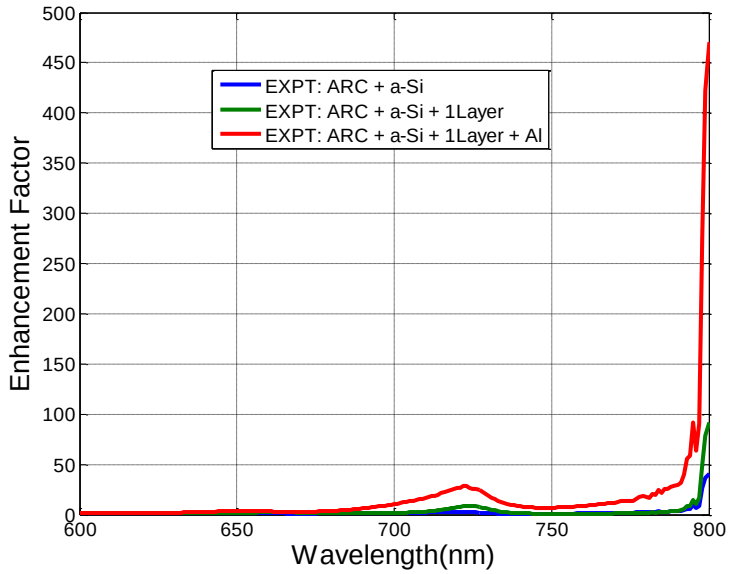

We see that the structure with the added aluminum layer, enhances the absorption by more than 400 times at about 800 nm wavelength. The average enhancement factor characteristics for all the structures considered in this study are tabulated in Table 5.

Table 5. Enhancement factor of the different design structures considered in this study.

Structure	Enhancement Factor (400–800 nm)	Enhancement Factor (600–800 nm)
a-Si Only	1	1
ARC + a-Si	1.8	2.1
ARC + a-Si + 1 Layer	2.4	3.4
ARC + a-Si + 1 Layer + Al	9	16

Finally, to put this work into greater context, we calculate what the short circuit current characteristics, J_{sc}, would be for the fabricated structures. The J_{sc} is given by Equation (4):

$$J_{\mathrm{sc}} = \frac{q}{hc}\int_{\lambda} \lambda' A(\lambda')Irrd(\lambda')\mathrm{d}\lambda' \quad (4)$$

where J_{sc} is the short circuit current density, q is the charge on an electron, h is Planck's constant, c is the speed of light, λ is the wavelength, A is the absorption of the silicon structure and *Irrd* is the solar irradiance spectrum [9,10,41]. It is worthwhile to note that in this calculation the conversion efficiency is taken to be one, we do not consider the internal carrier collection efficiency, and hence this gives the upper-bound of the current that can be collected from such a structure. The J_{sc} results are tabulated in Table 6, and plotted in Figure 17.

Table 6. Short circuit current characteristics (J_{sc}) of the different design structures considered in this study.

Structure	J_{sc} (mA/cm^2) (400–800 nm)
a-Si Only	9.4
ARC + a-Si	13.2
ARC + a-Si + 1 Layer	14
ARC + a-Si + 1 Layer + Al	19.3
Maximum J_{sc}	25.6

Figure 17. Plot of short circuit current characteristics (J_{sc}) of the different design structures considered in this study.

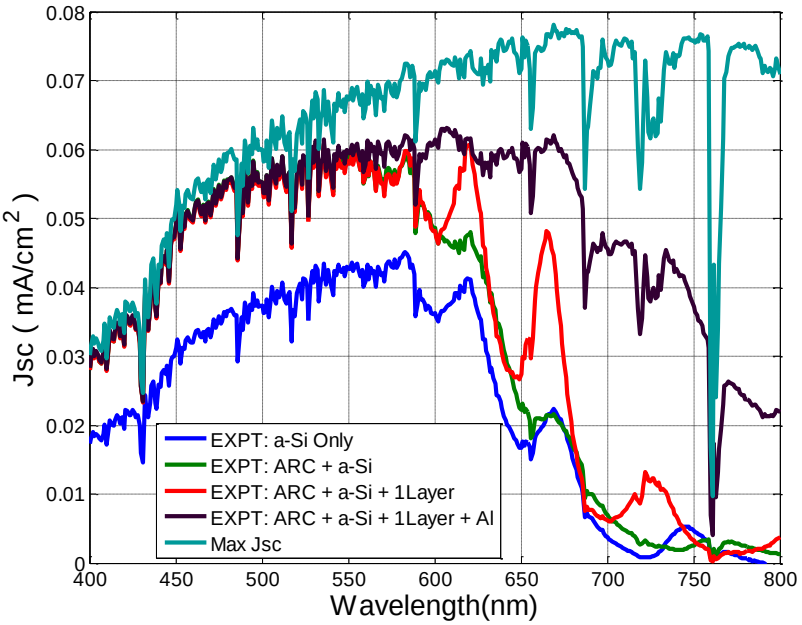

We also simulated the performance of the structure under illumination at different angles of incidence; we started from zero degrees and went all the way up to 40 degrees, with increments of 10 degrees in between. The results from this study are shown in Figure 18 and Table 7. We see that the absorption increases as the incident angle is increased; this is a good sign of the versatility of the structure.

Figure 18. Absorption characteristics of the structure with an AR coating, 1 Layer DBR and an aluminum layer, at different angles of incidence. This graph shows the performance at an incidence angle of 0, 10, 20, 30 and 40 degrees. We see that the performance is even better at larger angles of incidence.

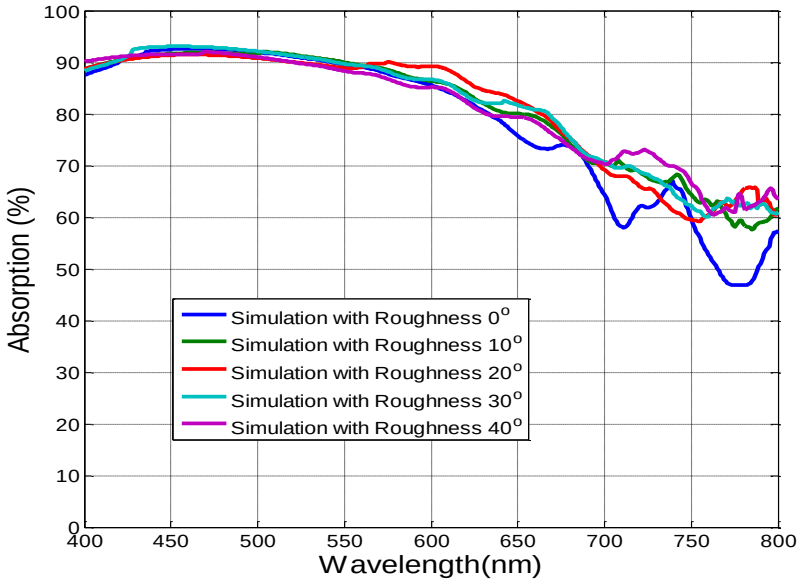

Table 7. Study of the performance of the structure with an AR coating, 1 Layer DBR and an aluminum layer, at different angles of incidence.

Incident Angle (in degrees)	Avg. Absorption for ARC + a-Si + 1 Layer + Al Structure
0	80.2
10	82
20	82.2
30	82.4
40	82

6. Conclusions

In this study, we have shown that we can indeed reduce the number of layers in a DBR stack to a single period, while still maintaining high back surface reflectance characteristics. This is accomplished by the addition of a metallic and a phase matching dielectric layer. We have also shown that the absorption of such a back reflector is minimal; about 2.3% of the incident light gets absorbed in such a reflector. In addition, we experimentally realized the structures and, as expected, saw increased absorption characteristics. However, the aluminum layer introduced roughness into the final fabricated structure and hence, served to heighten the absorption characteristics beyond what we had initially expected in theory. This study also concluded that the final structure performs well under obliquely incident illumination, the absorption characteristics actually increased with the increased angles of incidence.

Acknowledgements

We would like to thank Jonathan Boyle for his assistance with spectrophotometer measurements.

References

1. *United Nations Framework Convention on Climate Change 2010*; United Nations. Available online: http://unfccc.int/2860.php (accessed on 8 December 2010).
2. Hegedus, S. Thin Film Solar Modules: The Low Cost, High Throughput and Versatile Alternative to Si Wafers. *Prog. Photovolt. Res. Appl.* **2006**, *14*, 393–411.
3. Hegedus, S.; Luque, A. Status, Trends, Challenges and the Bright Future of Solar Electricity from Photovoltaics. In *Handbook of Photovoltaic Science and Engineering*; Luque, A., Hegedus, S., Eds.; John Wiley & Sons, Inc.: Chichester, UK, Hoboken, NJ, USA, 2003; pp. 1–43.
4. Green, M.A.; Emery, K.; Hishikawa, Y.; Warta, W. Solar Cell Efficiency Tables (Version 36). *Prog. Photovolt. Res. Appl.* **2010**, *18*, 346–352.
5. Hecht, E. *Optics*, 4th ed.; Addison Wesley: Reading, MA, USA, 2001.
6. Mutitu, J.G.; Shi, S.; Chen, C.; Barnett, A.; Honsberg, C.; Prather, D.W. Light Trapping Designs for Thin Silicon Solar Cells Based on Photonic Crystal and Metallic Diffractive Grating Structures. In *Proceedings of the 34th IEEE Photovoltaic Specialists Conference*, Philadelphia, PA, USA, June 2009.
7. Mutitu, J.G.; Shi, S.; Chen, C.; Barnett, A.; Honsberg, C.; Prather, D.W. Light Trapping Designs for Thin Film Silicon Solar Cells. Presented at IGERT Solar Hydrogen Conference, Newark, DE, USA, 2008.
8. Macleod, H.A. *Thin-Film Optical Filters*, 2nd ed.; Macmillan Publishing Company: New York, NY, USA; Adam Hilger Ltd.: Bristol, UK, 1986.
9. Mutitu, J.G.; Shi, S.; Barnett, A.; Prather, D.W. Angular Selective Light Filter Based on Photonic Crystals for Photovoltaic Applications. *IEEE Photonics J.* **2010**, *2*, 490–499.
10. Mutitu, J.G.; Shi, S.; Chen, C.; Creazzo, T.; Barnett, A.; Honsberg, C.; Prather, D.W. Thin Film Silicon Solar Cell Design Based on Photonic Crystal and Diffractive Grating Structures. *Opt. Express* **2008**, *16*, 15238–15248.
11. Banerjee, A.; Guha, S. Study of Back Reflectors for Amorphous Silicon Alloy Solar Cell Application. *J. Appl. Phys.* **1991**, *69*, 1030–1035.
12. Hegedus, S.S.; Kaplan, R. Analysis of Quantum Efficiency and Optical Enhancement in Amorphous Si p-i-n Solar Cells. *Prog. Photovolt. Res. Appl.* **2002**, *10*, 257–269.
13. Hegedus, S.; Sopori, B.; Paulson, P.D. Optical Design and Analysis of Textured a-Si Solar Cells. In *Proceedings of the 29th IEEE Photovoltaic Specialists Conference*, New Orleans, LA, USA, May 2002; pp. 1122–1125.
14. Meier, J.; Spitznagel, J.; Kroll, U.; Bucher, C.; Fay, S.; Moriarty, T.; Shah, A. Potential of Amorphous and Microcrystalline Silicon Solar Cells. In *Proceedings of the Symposium D on Thin Film and Nano-Structured Materials for Photovoltaics of the E-MRS 2003 Spring Conference*, Strasbourg, France, March 2003; pp. 518–524.

15. Müller, J.; Rech, B.; Springer, J.; Vanecek, M. TCO and Light Trapping in Silicon Thin Film Solar Cells. *Sol. Energy* **2004**, *77*, 917–930.
16. Deng, X.; Schiff, E.A. Amorphous Silicon-based Solar cells. In *Handbook of Photovoltaic Science and Engineering*; Luque, A., Hegedus, S., Eds.; John Wiley & Sons, Inc.: Chichester, UK; Hoboken, NJ, USA, 2003; pp. 505–565.
17. Whittaker, D.M.; Culshaw, I.S. Scattering-Matrix Treatment of Patterned Multilayer Photonic Structures. *Phys. Rev. B: Condens. Matter Mater. Phys.* **1999**, *60*, 2610–2618.
18. Li, E.; Wang, Q.; Zhang, Y.; Ooi, B. Analysis of Finite-Size Coated Electromagnetic Bandgap Structure by an Efficient Scattering Matrix Method. *JSTQE* **2005**, *11*, 485–492.
19. Yonekura, J.; Ikeda, M.; Baba, T. Analysis of Finite 2-D Photonic Crystals of Columns and Lightwave Devices using the Scattering Matrix Method. *J. Lightwave Technol.* **1999**, *17*, 1500–1508.
20. Hu, X. Particle Swarm Optimization Home page. Available online: http://www.swarmintelligence.org (accessed on 8 December 2010).
21. Eberhart, R.; Shi, Y. Particle Swarm Optimization: Developments, Applications and Resources. In *Proceedings of the 2001 Congress on Evolutionary Computation*, Seoul, Korea, 2001; pp. 81–86.
22. Eberhart, R.; Kennedy, J. A New Optimizer using Particle Swarm Theory. In *Proceedings of the 6th International Symposium on Micromachine and Human Science*, Nagoya, Japan, 1995; pp. 39–43.
23. Zeng, L.; Yi, Y.; Hong, C.; Liu, J.; Feng, N.; Duan, X.; Kimerling, L.C.; Alamariu, B.A. Efficiency Enhancement in Si Solar Cells by Textured Photonic Crystal Back Reflector. *Appl. Phys. Lett.* **2006**, *89*, 111111.
24. Zhao, L.; Zuo, Y.H.; Zhou, C.L.; Li, H.L.; Diao, H.W.; Wang, W.J. A Highly Efficient Light-Trapping Structure for Thin-Film Silicon Solar Cells. *Sol. Energy* **2010**, *84*, 110–115.
25. Zhou, D.; Biswas, R. Photonic Crystal Enhanced Light-Trapping in Thin Film Solar Cells. *J. Appl. Phys.* **2008**, *103*, 093102-5.
26. Biswas, R.; Dayu, Z. Enhancing Light-Trapping and Efficiency of Solar Cells with Photonic Crystals. In *Proceedings of the 2007 MRS Spring Meeting*, San Francisco, CA, USA, April 2007; pp. 35–40.
27. Bermel, P.; Luo, C.; Zeng, L.; Kimerling, L.C.; Joannopoulos, J.D. Improving Thin-Film Crystalline Silicon Solar Cell Efficiencies with Photonic Crystals. *Opt. Express* **2007**, *15*, 16986–17000.
28. Feng, N.; Michel, J.; Zeng, L.; Liu, J.; Hong, C.; Kimerling, L.C.; Duan, X. Design of Highly Efficient Light-Trapping Structures for Thin-Film Crystalline Silicon Solar Cells. *IEEE Trans. Electron Devices* **2007**, *54*, 1926–1933.
29. Tobias, I.; Luque, A.; Marti, A. Light Intensity Enhancement by Diffracting Structures in Solar Cells. *J. Appl. Phys.* **2008**, *104*, 034502-1.
30. Heine, C. Submicrometer Gratings for Solar Energy Applications. *Appl. Opt.* **1995**, *34*, 2476–2482.
31. Ferry, V.E.; Verschuuren, M.A.; Li, H.B.T.; Verhagen, E.; Walters, R.J.; Schropp, R.E.I.; Atwater, H.A.; Polman, A. Light Trapping in Ultrathin Plasmonic Solar Cells. *Opt. Express* **2010**, *18*, A237–A245.
32. Catchpole, K.R.; Polman, A. Plasmonic Solar Cells. *Opt. Express* **2008**, *16*, 21793–21800.

33. Yang, Z.; Ci, L.; Bur, J.A.; Lin, S.; Ajayan, P.M. Experimental Observation of an Extremely Dark Material made by a Low-Density Nanotube Array. *Nano Lett.* **2008**, *8*, 446–451.
34. Zhu, J.; Hsu, C.; Yu, Z.; Fan, S.; Cui, Y. Nanodome Solar Cells with Efficient Light Management and Self-Cleaning. *Nano Lett.* **2010**, *10*, 1979–1984.
35. Zhu, J.; Yu, Z.; Burkhart, G.F.; Hsu, C.; Connor, S.T.; Xu, Y.; Wang, Q.; McGehee, M.; Fan, S.; Cui, Y. Optical Absorption Enhancement in Amorphous Silicon Nanowire and Nanocone Arrays. *Nano Lett.* **2009**, *9*, 279–282.
36. Sopori, B.; Madjdpour, J.; Zhang, Y.; Chen, W.; Guha, S.; Yang, J.; Banerjee, A.; Hegedus, S. Optical Modeling of a-Si Solar Cells. In *Proceedings of the Materials Research Society's Spring 1999 Meeting*, San Francisco, CA, USA, April 1999; pp. 755–760.
37. Sopori, B.L.; Madjdpour, J.; Von Roedern, B.; Chen, W.; Hegedus, S.S. Optical Losses in Amorphous Silicon Solar Cells due to Back Reflectors. In *Amorphous and Microcrystalline Silicon Technology*, Proceedings of the 1997 Symposium of Materials Research Society, Pittsburgh, PA, USA, March–April 1997; pp. 777–782.
38. Balanis, C. *Advanced Engineering Electromagnetics*; John Wiley & Sons, Inc.: Chichester, UK, Hoboken, NJ, USA, 1989.
39. Park, K.C. The Extreme Values of Reflectivity and the Conditions for Zero Reflection from Thin Dielectric Films on Metal. *Appl. Opt.* **1964**, *3*, 877–881.
40. Rakic, A.D.; Djurisic, A.B.; Elazar, J.M.; Majewski, M.L. Optical Properties of Metallic Films for Vertical-Cavity Optoelectronic Devices. *Appl. Opt.* **1998**, *37*, 5271–5283.
41. Brendel, R.; Goetzberger, A. *Thin-Film Crystalline Silicon Solar Cells: Physics and Technology*; Wiley-VCH Verlag GmbH & Co. KGaA: Weinheim, Germany, 2003.